 CMC, vol.16, no.2, pp.101-115, 2010

A Molecular Dynamics Study of Irradiation Induced Cascades in Iron Containing Hydrogen

E. Hayward[1] **and C. Deo**[1]

Abstract: Damage cascades representative of those that would be induced by neutron irradiation have been simulated in systems of pure iron and iron containing 0.01 at.% hydrogen. Results from molecular dynamics simulations using three different embedded-atom method (EAM) type potentials are compared for primary knock-on atom energies of 5, 10, and 20 keV to assess the effect of hydrogen on the primary damage state. We examine the influence of hydrogen on the primary damage state due to a single radiation cascade. These results can serve as an atomistic database for methods and simulations for long time scale evolution of radiation damage.

Keywords: Molecular dynamics, damage cascade, irradiation, iron, hydrogen, nuclear.

1 Introduction

In this paper, we investigate the primary damage state created in iron with and without hydrogen interstitials due to irradition by neutrons of varying energies. Body centered cubic (bcc) iron is of interest because it is the primary component of ferritic steels used for light water reactor pressure vessels, fuel cladding, and coolant tubes. Macroscopic properties, such as plasticity, hardness, brittleness, and creep behavior, of structural steels may change due to microstructural effects of radiation. Atomistics can be a useful tool to generate data about the structure and development of defects, on length and time scales that experiments can not probe.

Hydrogen is introduced to reactor structural materials by transmutation, deposition, or diffusion, and is known to affect macroscopic stability of steel by forming bubbles which may cause embrittlement. In a tokamak, the isotopes deuterium and tritium are constantly bombarding and being retained in the first wall. Hydrogen

[1] Nuclear and Radiological Engineering Program, George W. Woodruff School of Mechanical Engineering, Georgia Institute of Technology, Atlanta, GA, 30332, USA. *erin@gatech.edu*.

typically has a low solubility, less than $3x10^{-6}$ at.%, in bulk iron at room temperature, however the solubility may be increased under certain conditions. Hydrogen may segregate to defects existing in materials due to manufacturing or irradition, such as grain boundaries and dislocations, resulting in higher concentrations.

1.1 Basics of Radiation Damage

Radiation damage occurs when incident particles transfer some or all of their energy to atoms in a solid, resulting in a change to the original structure. The process involves several steps. First, the incident radiation has an interaction with an atom in the crystal lattice, transferring enough energy to remove the atom from its site. This atom, the primary knock-on atom (PKA), goes on to interact with other atoms in the crystal, removing them from their sites and generating a displacement cascade in the thermal spike phase. Thus Frenkel pair defects (equal number of vacancies and interstitials) are created. At some time shortly after the PKA is created, some peak number of Frenkel pairs N_p will exist in the crystal, where a Frenkel pair is defined as one vacancy plus one interstitial. A profile of the number of defects over time in a typical cascade can be seen in Figure 1. The figure shows the number of Frenkel pairs plotted as a function of time. Initially the PKA produces a large number of Frenkel pairs as it knocks atoms off their lattice site. After this point, the defects will begin to recombine as the energy is dissipated. As time progress, these atoms rearrange on crystalline lattice sites, reducing the number of defects. After a few picoseconds, only a few defects N_d will remain. This generally results in a core of vacancies surrounded by a shell of interstitials. . More information on cascades can be found in Was (2007) and Stoller (1996).

The amount of energy that an incident particle can transfer to a lattice atom is a function of the mass of the particle, the mass of the atom, and the angle at which the collision occurs. Energy can be lost through inelastic collisions, (n, 2n) or (n, γ) reactions, and, most importantly, elastic collisions. Elastic collisions between neutrons and nuclei can be treated within the hard sphere model with the following equations:

$$T = \frac{\gamma}{2} E_i (1 - \cos\phi) \tag{1}$$

$$\gamma = \frac{4A}{(1+A)^2}, \tag{2}$$

where T is the total energy transferred, E_i is the energy of the incident neutron, ϕ is the angle of collision, and A is the mass of the lattice nucleus. With the assumption that scattering is isotropic in the center of mass system, the average energy transferred over all angles can be shown to be the average of the minimum and

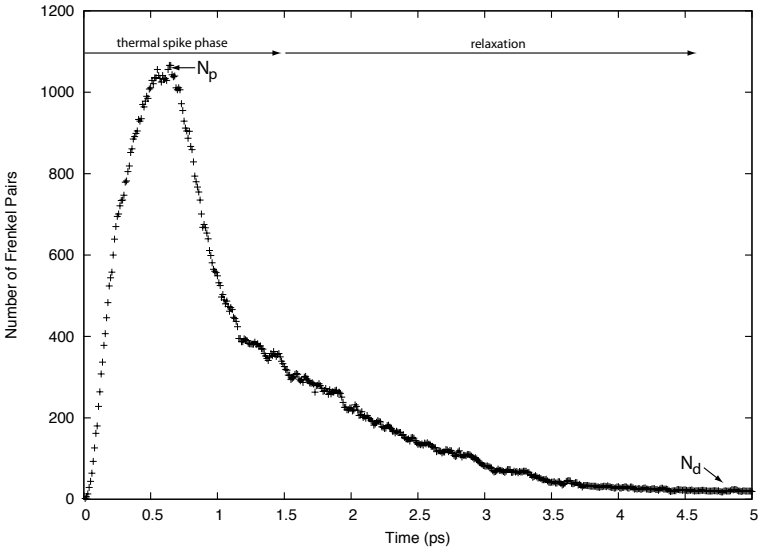

Figure 1: Number of frenkel pairs (vacancy and interstitial) as a function of time (ps). Initial peak in defect concentration occurs during the thermal spike phase, many defects recombine in the subsequent relaxation over several picoseconds.

maximum possible transfer energies, so

$$\bar{T} = \frac{\gamma E_i}{2}. \tag{3}$$

For iron, the energy required to displace an atom off its lattice site is about 40 eV (depending on the direction from which it is struck), so a neutron needs a minimum energy of about 581 eV to displace an iron atom. Neutrons produced from fission of uranium carry around 2 MeV of kinetic energy and so have potential to cause damage as they slow down. Additionally, deuterium-tritium fusion reactions produce neutrons with energy of 14.1 MeV.

The first attempt to create a model for defect production based on PKA energy comes from Kinchen and Pease (1955). In this model, above a certain threshold, energy is lost only to electron excitation, while below it, energy is lost only in hard-sphere elastic scattering. Norgett, Robinson and Torrens (1975) proposed a revised model, taking into account a more realistic energy transfer cross section, based on binary collision model simulations:

$$N_d^{NRT} = \frac{0.8E_D}{2E_d}. \tag{4}$$

N_d is the number of Frenkel pairs surviving relaxation and the damage energy E_D is the amount of energy available for creating displacements through elastic collisions and is a function of T. Since some of the energy of the cascade is lost to electronic excitation E_D will be less than T; for the energy range considered in this paper, E_D can be estimated as equal to T. This model is frequently used as the standard for estimating displacements per atom (dpa) which is a standard means to describe radiation damage in crystalline materials. Many molecular dynamics simulations have shown that the NRT equation (Equation 4) tends to strongly overestimate the actual damage efficiency. Bacon, Gao and Osetsky (2000) proposed an empirical relationship between N_d and T given by:

$$N_d^{BGO} = AT^n \tag{5}$$

where A and n are weakly temperature dependent constants fit to particular materials, respectively equal to 5.57 and 0.83 for Fe at 100 K, and T is in keV.

1.2 Existing Work

The study of irradiation damage cascades has been a popular topic over the last fifteen or so years. A through literature review of the many different of damage cascade simulations, such as binary collision approximation and kinetic Monte Carlo, that have been performed in a variety of materials is beyond the scope of this paper and readers are referred to Was (2007). The following brief review will concentrate solely on molecular dynamics simulations in α-Fe.

A thorough review of results from many papers was written by Malerba (2006) who cites the first published molecular dynamics study in α-iron as being performed by Calder and Bacon (1993). Eighty cascades with PKAs of up to 5 keV were analyzed for properties such as percent of defects surviving relaxation, channeling properties, temperature dependence, and clustering. The interatomic potential used was developed by Finnis and Sinclair (1984) and stiffened by Calder and Bacon to treat small interatomic distance properly. This article established a large base of data for future papers to compare with.

Several similar studies using molecular dynamics followed this initial study. These studies utilized both the modified FS potential mentioned above and competing multi-body potentials including those from Haftel, Andreadis, Lill and Eridon (1990), Johnson and Oh (1989), Harrison, Voter and Chen (1989), and Simonelli, Pasianot and Savino (1994). These papers had three main motivations: to generate data from a new potential, to compare data between two or more potentials, or to compare damage in α-Fe with that in another material such as copper. The main difficulties in comparing results from different authors are defining what makes up a cluster of defects and non-reporting of exactly how cascades were generated.

Many authors contributed to generate databases; some papers of note are described here. Stoller, Odette and Wirth (1997), using the FS potential modified by Calder and Bacon, ran a number of cascades at energies up to 40 keV. They found evidence for vacancy clustering, a feature not seen in previous works. Bacon, Gao and Osetsky (2000) performed a study comparing the cascade characteristics of bcc, hcp, and fcc metals. They found that there were no major differences in interstitial and vacancy production, so they concluded that any differences observed experimentally must be due to evolution of the microstructure following the primary damage event. Caturla, Soneda, Alonso, Wirth, de la Rubia and Perlado (2000) compared bcc Fe with fcc Cu, finding that clustering in Fe was at least an order of magnitude less than in Cu. Terentyev, Lagerstedt, Olsson, Nordlund, Wallenius, Becquart and Malerba (2006) produced a study looking solely at differences between four available potentials by applying the same defect counting criteria to each. They found that the stiffness of a potential, a somewhat arbitrary feature, was the most important factor in determining cascade properties.

Despite this wealth of information for pure iron, the authors are unaware of any study of cascades in iron containing hydrogen. This is possibly due to the lack of availability of a suitable potential for Fe-H until recently.

2 Computational Details

All cascade simulations were performed using LAMMPS (Plimpton (1995)). PKA energies of interest were 5, 10, and 20 keV; this is equivalent to energy transferred, T. Following from Equation 1, a PKA will be given energy T when it scatter with a neutron of energy E_i at angle ϕ. One molecular dynamics calculation at energy T is representative of a range of possible combinations of neutron energy and collision angle; these are shown in Figure 2.

For the pure Fe cascades, the embedded atom method (EAM) potential #2 from Mendelev, Han, Srolovitz, Ackland, Sun and Asta (2003) was used. This potential was generated by fitting to first-principles forces seen in the liquid state in addition to bulk crystal data and crystal defect information. Using data from a liquid-like state lets this potential give a better description of interaction at small separations than had been seen in previous iron potentials, due to the fact that atoms in liquid iron will often find themselves closer together than atoms in a solid; this is also the situation with interstitials in iron. As evidence of the effectiveness of this fitting method, this potential predicts the formation energies of interstitial dumbbells very accurately (within 3%) despite not having been fit to these parameters directly. By comparison, a potential generated by Ackland, Bacon, Calder and Harry (1997) that was fit to all the same parameters, except the liquid state, overestimates these energies by up to 40% in some directions.

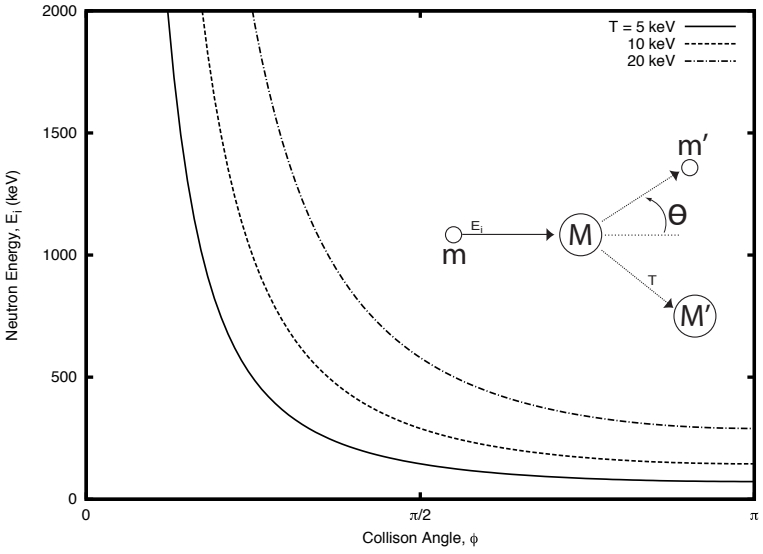

Figure 2: $E_i = 2T/[\gamma(1-\cos\phi)]$ for PKA energies simulated in this study, where γ=0.069. Center-of-mass scattering angle ϕ can be related to laboratory scattering angle by $\tan\theta = \frac{(M/m)\sin\phi}{1+(M/m)\cos\phi}$.

Two Fe-H potentials, which were developed by Ramasubramaniam, Itakura and Carter (2009), were used for comparison. The first, hereafter referred to as potential A, takes the Fe-Fe interactions from potential #4 of the above mentioned Mendelev work. This iron potential is similar to #2, however it is fit to experimental liquid structure data instead of first-principles calculations of liquid states. The two potentials give very close results for a number of physical properties, including lattice parameter, elastic constants, and vacancy formation energy. One difference worth noting is that potential #4 predicts interstitial dumbbell formation energies 9-13% lower than does potential #2. However, the ordering of the directionality of the dumbbells is consistent; both potentials predict dumbbells in the <1 1 0> direction to have the lowest formation energy, followed by the <1 1 1> and <1 0 0> directions.

The second Fe-H potential, hereafter referred to as potential B, gets its Fe-Fe interactions from a 2004 potential from Ackland, Mendelev, Srolovitz, Han and Barashev (2004). This potential is simply a slightly improved version of the Mendelev, Han, Srolovitz, Ackland, Sun and Asta (2003) potential #2, fitted to eliminate negative thermal expansion.

In order to fit the Fe-H and H-H interactions, Ramasubramaniam, Itakura and

Table 1: For each PKA energy simulated (T, second column), the average neutron energy ($\bar{E}_i$), the size of the simulation cell (in units of the bcc Fe lattice spacing a_0) and the corresponding number of iron atoms in the simulation (N_{Fe}) are tabulated.

$\bar{E}_i$ (keV)	T (keV)	Size (a_0)	N_{Fe}
145.1	5	50	250,000
290.3	10	60	432,000
580.6	20	100	2,000,000

Carter (2009) used a variant of the EAM and Finnis-Sinclair (FS) formalisms to describe the total energy of the system. Using this general many-body form, the two-body interactions and electron densities are specified independently for each type of interaction. Data from first-principles DFT was used for fitting. Specifically, dissolution and binding energies for various configurations in the bulk and in the presence of vacancies were considered. A battery of tests were run by Ramasubramaniam to assess the performance of the potentials for a variety of situations and results were in good agreement with DFT predictions. It should be noted that two additional potentials were developed by additionally fitting to surface data, but these potentials have inferior performance in the bulk, so they are not considered in this study.

Periodic boundary conditions were employed, so care was taken to ensure the simulation boxes were large enough to avoid image effects. Cascades were visually inspected to check for self-interference; in addition, test runs were performed with larger boxes to make sure the number of defects seen was representative of a cascade in an infinite medium. As neutron energies increase, larger simulation box sizes are needed. Table 1 shows the dimensions of the simulation boxes for the various PKA energies studied and the average neutron energy that would generate a PKA with energy T, as follows from Equation 3.

For the pure iron cascades, the simulation box was filled with perfect bcc lattice. For the hydrogen cascades, an appropriate number of tetrahedral interstitial sites (Jiang and Carter (2004)) were randomly selected to hold H atoms; every regular bcc site still contained an iron atom. The solubility of hydrogen is 0.01 at.% at 1000 K, and significantly lower at room temperature. Even though the simulations in this paper were run at 300 K, the above mentioned solubility was used with the assumption that in an operating reactor environment, in particular in a tokamak, more hydrogen may be implanted than would normally be soluble.

In order to simulate damage from a neutron hitting the bulk, a random atom near the center of the simulation box was chosen to be the primary knock-on atom. This atom was given a velocity corresponding to the desired cascade energy. The

molecular dynamics algorithm then proceeded to integrate Newton's equations of motion for all atoms Rapaport (2004).

At the beginning of each simulation, equilibration of the lattice was performed at 300 K for 10 ps. A damped Nose-Hoover thermostat was used with a NVT ensemble, in which the number of atoms, volume of the box, and the temperature are kept constant. Before equilibration, the Fe-H systems were minimized with conjugate gradient methods to allow the atoms neighboring the H interstitials to relax. For pure iron, a relatively large timestep of 10 fs was employed for this stage of the simulation since atoms would not be moving very far. The Fe-H systems were more sensitive, so a timestep of 1 fs was chosen.

The representative direction initially imparted to the PKA has been a subject of study in the past (Was (2007)). Cascades were induced in the <1 3 5> direction. This direction is often used in the literature to be representative of a random direction; it also has the benefit that it reduces channeling. 1 keV simulations were performed this direction in pure Fe, as well as in the <1 0 0>, <1 1 0>, and <1 1 1> directions to verify this claim. Six cascade simulations were performed in each direction, in a box which had been equilibrated at 100 K. The average and the standard deviation of the number of Frenkel pairs created for each direction was compared. The results of this test can be seen in Figure 3. Each datapoint indicates the average number of Frenkel pairs for each direction and the vertical error bar showing the standard deviation in terms of the number of Frenkel pairs created. It can be seen that the <1 3 5> direction is indeed representative of a random direction as is chosen to be the PKA direction for our simulations.

The thermal spike phase begins with the introduction of the PKA. During this phase a microcanonical ensemble (NVE) was used, in which the number of atoms, volume of the box, and total energy are conserved. No further attempt was made to keep the box at 300 K.

Five picoseconds after the cascade is induced, the crystal has begun to anneal significantly through recombination of defects. For the 5 keV cascades, relaxation is performed for 5 more ps; for the 10 and 20 keV cascades, relaxation continues for 20 ps.

At any point in time, the simulation cell contains the atoms distributed in accordance with the MD prescription. However this is in the form of atom positions. We are interested in the location and number of defects (vacancies, interstitials). We have developed a post-processing tool, utilizing the Wigner-Seitz supercell method Kittel (1953), for counting the number of Frenkel pairs at different stages in the cascade. This method is a popular one because the entire simulation box is covered; methods that count defects based on distance from lattice sites may miss areas

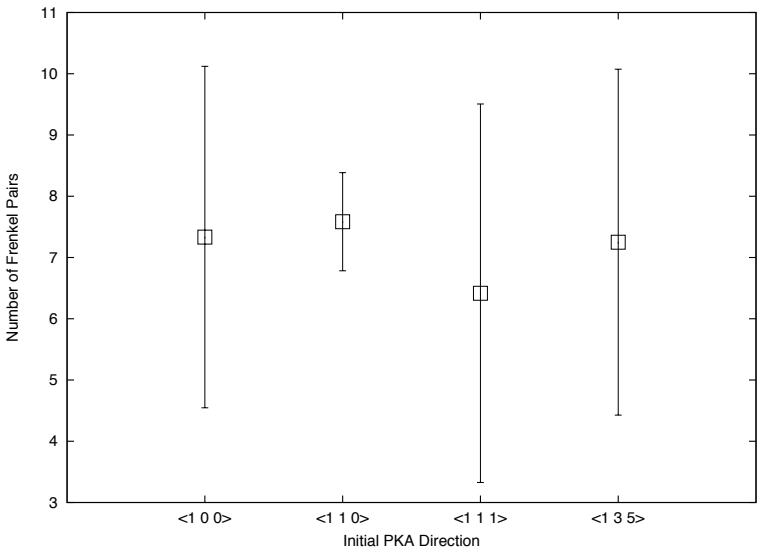

Figure 3: The number of Frenkel pairs created as a function of the initial direction of the primary knock on atom (PKA). This serves to provide a comparison of PKA initial directions for 1 keV cascades. The datapoint show the average number of Frenkel pairs while the error bars show the standard deviation.

of the box. Our technique is described below.

First, the simulation box is broken up into cubic supercells, corresponding in size and shape to, but offset from the unit lattice cubes by $\frac{1}{4}a_0$ in the x, y, and z directions. This offsetting is necessary to avoid miscounting of defects as the atoms oscillate around their lattice sites due to thermal motion. A schematic can be seen in Figure 4.

At $t = 0$, the supercells record how many iron atoms are within their bounds; this is two for a perfect bcc lattice. During the cascade simulation, atoms positions are recorded every n timesteps. For each of these timesteps, the code again calculates the number of iron atoms within supercell bounds and compares this number to the number at initialization. A cell is identified as having vacancies, if there are less than two atoms in the cell, or interstitials, if there are more than two atoms in the cell.

3 Results

At least eight, and as many as twenty, independent simulations were performed to generate the data for each combination of potential and PKA energy to ensure

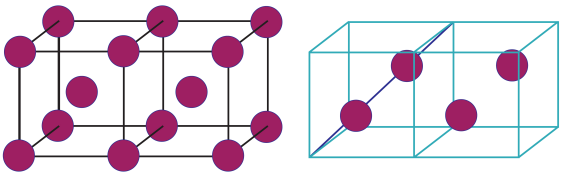

Figure 4: Illustration of the Wigner Sitz cell for the bcc lattice. On the left is the standard pictoral representation of the bcc unit cell, on the right is the corresponding Wigner Sitz cell.

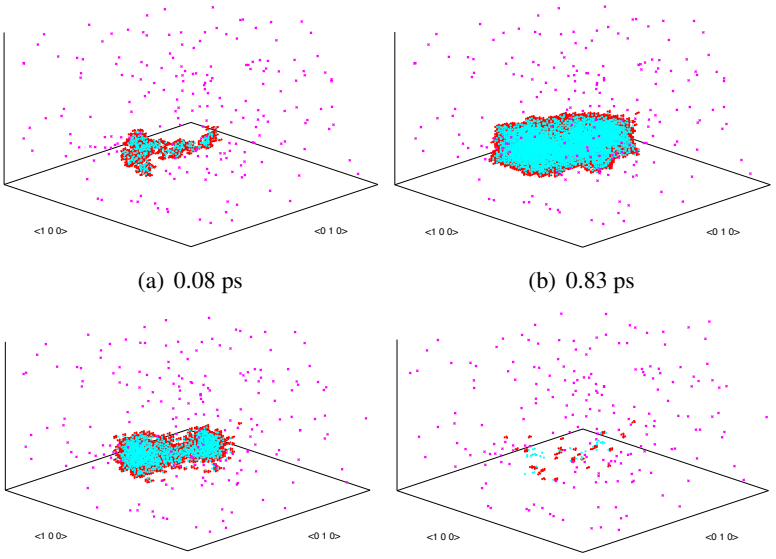

(a) 0.08 ps (b) 0.83 ps

(c) 2.0 ps (d) 12.0 ps

Figure 5: Snapshots from a T=20 keV cascade. Blue/light grey dots are vacancies, red/dark grey dots are self-interstitials, and crosses are hydrogen atoms.

Table 2: Data on number of defects. T is the initial PKA energy, $\bar{N}_p$ is the average number of defects at peak time, $\bar{N}_d$ is the average number of defects remaining after relaxation, and $\sigma(N_d)$ is the standard deviation of the number of surviving defects. System refers to the interatomic potential employed.

T	System	$\bar{N}_p$	$\bar{N}_d$	$\sigma(N_d)$	N_d^{NRT}	N_d^{BGO}
5 keV	Fe	969.30	16.57	6.14	50	21.2
	Fe-H (A)	794.15	12.14	3.33		
	Fe-H (B)	905.30	18.67	5.17		
10 keV	Fe	2700.10	26.24	10.96	100	37.7
	Fe-H (A)	2369.89	20.98	7.99		
	Fe-H (B)	2556.22	27.90	11.20		
20 keV	Fe	6018.33	55.91	15.10	200	66.9
	Fe-H (A)	6076.44	39.24	4.58		
	Fe-H (B)	6710.63	62.36	11.02		

that sufficient statistics were gathered. Results from individual cascade simulations tend to be widely varied, so standard deviations are large. However, general trends can clearly be seen in our data. We have analyzed both raw defect counts, where a defect is defined as a Frenkel pair, at peak (N_p) and relaxed (N_d) times, as well as the fraction (expressed as a percentage) of defects that survive relaxation ($\xi = N_d/N_p$).

Table 2 shows raw data on the number of defects generated for each case, as well as comparisons with the number of defects predicted by NRT (Norgett, Robinson and Torrens (1975)) and BGO (Bacon, Gao and Osetsky (2000)) as described in Equations 4 and 5. In the 5 and 10 keV cases, the pure Fe simulations generated the most defects at peak time, while Fe-H potential A generated the least. After relaxation, potential A had the fewest remaining defects, potential B had the most, and pure Fe had numbers slightly below those of potential B. The same trend is seen for N_d at 20 keV. However, at 20 keV pure iron has the smallest number of defects at peak time.

NRT predictions of defect numbers are extremely high, as has been seen previously in the literature. For pure Fe and potential B, $\bar{N}_d$ is below, but reasonably close to, BGO predictions. This discrepancy may be due to the fact that our simulations were run at 300 K, while Equation 5 is optimized for 100 K simulations. Its predictions are expected to be slightly lower at higher temperatures.

The same trends are followed for the data on the percentage of defects that survive relaxation, shown in Table 3. For 5 and 10 keV, potential A has the smallest percent surviving, followed by pure Fe, then potential B with the largest percent surviving.

Table 3: Data on percentage of defects surviving relaxation. T is initial PKA energy, $\bar{\xi}$ is the average percent surviving relaxation, and $\sigma(\xi)$ is the standard deviation of this number. System refers to the interatomic potential employed.

T	System	$\bar{\xi}$ (%)	$\sigma(\xi)$ (%)
5 keV	Fe	1.78	0.80
	Fe-H (A)	1.65	0.83
	Fe-H (B)	2.14	0.83
10 keV	Fe	1.05	0.61
	Fe-H (A)	0.92	0.38
	Fe-H (B)	1.28	0.83
20 keV	Fe	0.98	0.43
	Fe-H (A)	0.67	0.16
	Fe-H (B)	0.97	0.35

At 20 keV, pure Fe shows the highest average percent surviving by a very small margin, but when taking into account the error bar, may follow the same trend as is seen in the lower energies.

All three potentials show the same negative correlation between N_p and ξ; that is, simulations which generated a large number of defects at peak time tended to have a smaller percentage survive than those that had fewer peak defects. This trend was observed for all energies and is illustrated in Figure 6. A large N_p is equivalent to the PKA energy T being distributed among many atoms. This generally occurs when a cascade is limited in volume, with many Frenkel pairs being created in a centralized region. As the structure relaxes, there are more opportunities for recombination, so a smaller fraction of the defects created survive. At a given energy, cascades exhibiting more branching tended to have higher values of ξ.

The structure of the cascades at 5 keV was varied, with some cases showing essentially no branching. In comparison, at 20 keV all the cascades showed evidence of subcascade formation. Subcascades at higher energies look basically like primary low energy cascades, and many 20 keV cascades exhibited multiple branches. It is reasonable to think of a 20 keV cascade as an average of a few low energy cascades occuring in a limited volume. Thus, the range of ξ is observed to be much smaller for higher energies than for lower energies, as the effects of branching are smeared out.

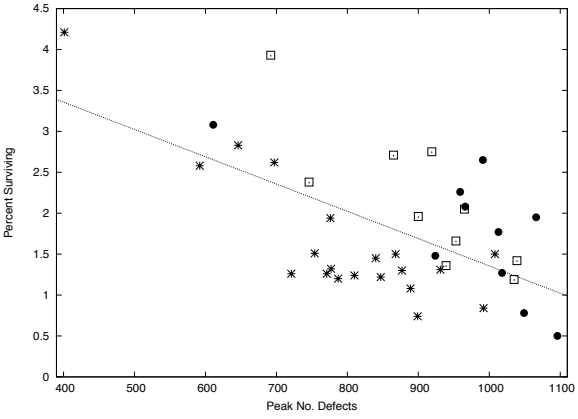

(a) 5 keV

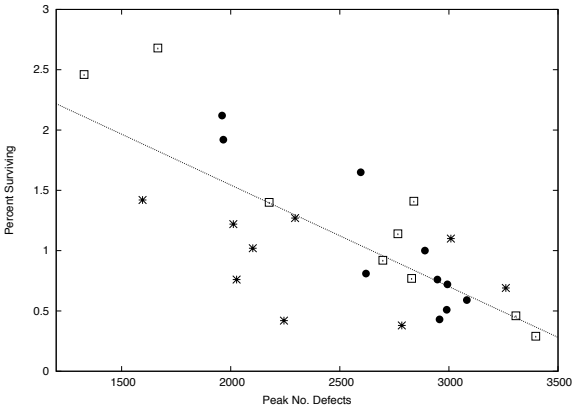

(b) 10 keV

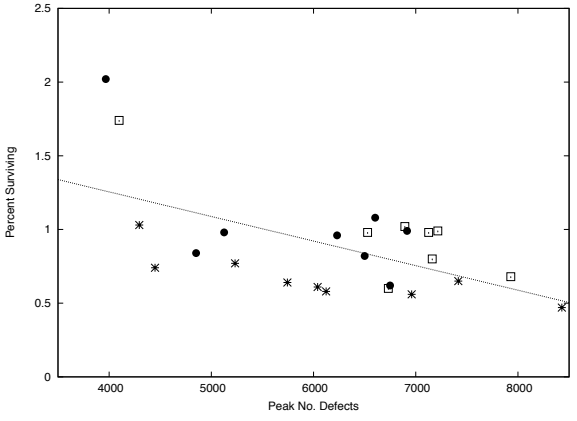

(c) 20 keV

Figure 6: Peak defects vs percentage surviving. Note differences in scale. Filled circles represent pure iron potential, stars Fe-H potential A, and hollow boxes Fe-H potential B; lines are linear regression fit.

4 Discussion and Conclusion

The primary damage state in pure iron and iron-hydrogen systems was simulated using three different EAM potentials. There is no clear effect of the studied concentration of hydrogen on the primary damage state in bcc iron on the timescale of tens of picoseconds. Potential A showed that fewer defects were created and sustained in Fe-H systems than in pure iron, but potential B showed that more defects remained after relaxation. In general, the values for N_p, N_d, and ξ for pure iron simulations lie in between the values found with potentials A and B. This fact leads the authors to conclude that the variation in results across potentials tells us more about the differences in the Fe-Fe interactions than it does about the effect of hydrogen inventory. It would be instructive to compare results from simulations in Fe and Fe-H with potentials which generate identical Fe-Fe interactions. However, it is clear than any effects from the presence of this concentration of hydrogen on the primary damage state are small, if they exist at all.

These simulations can form an atomistic database on atomic positions for simulations that occur on longer timescales, including kinetic Monte Carlo and continuum modelling. Additionally, phase field models and two point correlation functions can benefit from the data gathered.

In conclusion, at the concentration of hydrogen in question, 0.01at.% H, there is no evidence that the primary damage state is significantly affected. This does not mean that the presence of hydrogen has no effect on the longterm evolution or behavior of the crystal; indeed, hydrogen is known to form voids and cause embrittlement of steels over long times. The timescale of the simulations presented is too short for notable diffusion of either hydrogen or self-interstial atoms, so clustering and void production was not observed. Future atomistic studies should be performed to explore the possible effects of hydrogen at varying concentrations and at higher temperatures, when hydrogen may diffuse fast enough to affect primary damage formation.

References

Ackland, G.; Bacon, D.; Calder, A.; Harry, T. (1997): Computer simulation of point defect properties in dilute fe-cu alloy using a many-body interatomic potential. *Philos Mag A*, vol. 75, no. 3, pp. 713–732.

Ackland, G.; Mendelev, M.; Srolovitz, D.; Han, S.; Barashev, A. (2004): Development of an interatomic potential for phosphorus impurities in alpha-iron. *Journal of Physics Condensed Matter*, vol. 16, pp. 2629–2642.

Bacon, D.; Gao, F.; Osetsky, Y. (2000): The primary damage state in fcc, bcc and hcp metals as seen in molecular dynamics simulations. *Journal of Nuclear Materials*, vol. 276, pp. 1–12.

Calder, A.; Bacon, D. (1993): A molecular-dynamics study of displacement cascades in alpha-iron. *Journal of Nuclear Materials*, vol. 207, pp. 25–45.

Caturla, M.; Soneda, N.; Alonso, E.; Wirth, B. D.; de la Rubia, T.; Perlado, J. (2000): Comparative study of radiation damage accumulation in cu and fe. *Journal of Nuclear Materials*, vol. 276, pp. 13–21.

Finnis, M.; Sinclair, J. (1984): A simple empirical n-body potential for transition metals. *Philosophical magazine. A. Physics of condensed matter. Defects and mechanical properties*, vol. 50, no. 1, pp. 45–55.

Haftel, M.; Andreadis, T.; Lill, J.; Eridon, J. (1990): Surface relaxation of alpha-iron and the embedded-atom method. *Physical Review B*, vol. 42, no. 18, pp. 11540–11552.

Harrison, R.; Voter, A.; Chen, S. (1989): Embedded atom potential for bcc iron. *Atomistic Simulation of Materials - Beyond Pair Potentials*, pp. 219–222.

Jiang, D.; Carter, E. A. (2004): Diffusion of interstitial hydrogen into and through bcc Fe from first principles. *Physical Review B*, vol. 70, no. 6, pp. 64102.

Johnson, R.; Oh, D. (1989): Analytic embedded atom method model for bcc metals. *J Mater Res*, vol. 4, no. 5, pp. 1195–1201.

Kinchen, G.; Pease, R. (1955): The displacement of atoms in solids by radiation. *Reports on Progress in Physics*, vol. 18, pp. 1–52.

Kittel, C. (1953): *Introduction to Solid State Physics*. John Wiley and Sons, Inc., seventh edition.

Malerba, L. (2006): Molecular dynamics simulation of displacement cascades in α-fe: a critical review. *Journal of Nuclear Materials*, vol. 351, no. 1-3, pp. 28–38.

Mendelev, M.; Han, S.; Srolovitz, D.; Ackland, G.; Sun, D.; Asta, M. (2003): Development of new interatomic potentials appropriate for crystalline and liquid iron. *Philosophical Magazine*, vol. 83, no. 35, pp. 3977–3994.

Norgett, M.; Robinson, M.; Torrens, I. (1975): A proposed method of calculating displacement dose rates. *Nucl Eng Des*, vol. 33, no. 1, pp. 50–54.

Plimpton, S. (1995): Fast parallel algorithms for short-range molecular dynamics. *J. Comp. Phys.*, vol. 117, pp. 1–19. http://lammps.sandia.gov.

Ramasubramaniam, A.; Itakura, M.; Carter, E. A. (2009): Interatomic potentials for hydrogen in α–iron based on density functional theory. *Physical Review B*.

Rapaport, D. (2004): *The Art of Molecular Dynamics Simulation*. Cambridge University Press, second edition.

Simonelli, G.; Pasianot, R.; Savino, E. (1994): Point-defect computer simulation including angular forces in bcc iron. *Physical Review B*, vol. 50, no. 2, pp. 727–738.

Stoller, R. (1996): Primary damage formation in irradiated materials. *JOM(USA)*, vol. 48, no. 12, pp. 23–27.

Stoller, R.; Odette, G.; Wirth, B. D. (1997): Primary damage formation in bcc iron. *Journal of Nuclear Materials*, vol. 251, pp. 49–60.

Terentyev, D.; Lagerstedt, C.; Olsson, P.; Nordlund, K.; Wallenius, J.; Becquart, C.; Malerba, L. (2006): Effect of the interatomic potential on the features of displacement cascades in alpha-fe: A molecular dynamics study. *Journal of Nuclear Materials*, vol. 351, no. 1-3, pp. 65–77.

Was, G. S. (2007): *Fundamentals of Radiation Materials Science: Metals and Alloys*. Springer.